NIS
53-89
5566
p. 23

N96-13429

SOFT X-RAY PROPERTIES OF THE BINARY MILLISECOND PULSAR J0437–4715

JULES P. HALPERN
Columbia Astrophysics Laboratory, Columbia University,
538 West 120th Street, New York, NY 10027
jules@carmen.phys.columbia.edu

CHRISTOPHER MARTIN
Downs Laboratory, California Institute of Technology, 220–47
Pasadena, CA 91125
cmartin@porgy.srl.caltech.edu

AND
HERMAN L. MARSHALL
Center for Space Research, Massachusetts Institute of Technology
37–667a, Cambridge, MA 02138
hermanm@space.mit.edu

Submitted to *The Astrophysical Journal*

Received _____; *accepted* _____

ABSTRACT

We obtained a light curve for the 5.75 ms pulsar J0437–4715 in the 65–120 Å range with 0.5 ms time resolution using the Deep Survey instrument on the *EUVE* satellite. The single-peaked profile has a pulsed fraction of 0.27 ± 0.05, similar to the *ROSAT* data in the overlapping energy band. A combined analysis of the *EUVE* and *ROSAT* data is consistent with a power-law spectrum of energy index $\alpha = 1.2-1.5$, intervening column density $N_{\rm H} = (5-8)\times 10^{19}$ cm^{-2}, and luminosity 5.0×10^{30} ergs s^{-1} in the 0.1–2.4 keV band. We also use a bright *EUVE/ROSAT* source only 4′.3 from the pulsar, the Seyfert galaxy RX J0437.4–4711 (= EUVE J0437–471 = 1ES 0435–472), to obtain an independent upper limit on the intervening absorption to the pulsar, $N_{\rm H} < 1.2 \times 10^{20}$ cm^{-2}.

Although a blackbody spectrum fails to fit the *ROSAT* data, two-component spectral fits to the combined *EUVE/ROSAT* data are used to limit the temperatures and surface areas of thermal emission that might make *partial* contributions to the flux. A hot polar cap of radius $50 - 600$ m and temperature $(1.0 - 3.3) \times 10^6$ K could be present. Alternatively, a larger region with $T = (4-12)\times 10^5$ K and area less than 200 km^2, might contribute most of the *EUVE* and soft X-ray flux, but only if a hotter component were present as well. Any of these temperatures would require some mechanism(s) of surface reheating to be operating in this old pulsar, the most plausible being the impact of accelerated electrons and positrons onto the polar caps. The kinematically corrected spin-down power of PSR J0437–4715 is only 4×10^{33} ergs s^{-1}, which is an order of magnitude less than that of the lowest-luminosity γ-ray pulsars Geminga and PSR B1055–52. The absence of high-energy γ-rays from PSR J0437–4715 might signify an inefficient or dead outer gap accelerator, which in turn accounts for the lack of a more luminous reheated surface such as those intermediate-age γ-ray pulsars may have.

Subject headings: pulsars: individual (PSR J0437–4715) – stars: neutron – X-rays: stars

1. INTRODUCTION

The 5.75 ms pulsar J0437–4715, discovered by Johnston et al. (1993), is the nearest millisecond pulsar at $d = 140$ pc, and is also in a 5.74 d binary orbit with a cool white dwarf companion of mass $\sim 0.2 M_\odot$ (Bailyn 1993; Bell, Bailes, & Bessell 1993; Danziger, Baade, & Della Valle 1993). Its radio emission is so bright that individual pulses are easily seen. It is also the only millisecond pulsar from from which pulsed X-rays have been detected (Becker & Trümper 1993), and one of two surrounded by a bow-shock nebula (Bell et al. 1993; 1995). Fundamental questions about PSR J0437–4715 and other millisecond pulsars are 1) whether or not its characteristic age, $P/2\dot{P}$, is consistent with the cooling age of its white dwarf companion, 2) whether its X-rays are magnetospheric in origin or thermally reheated surface emission, and 3) why it is not (yet) a detectable high-energy γ-ray source.

Accurate determinations of $\dot{P}$ and proper motion for PSR J0437–4715 have now been established (Bell et al. 1995; Bell 1995) that will have a major impact upon all of these mysteries. Its intrinsic $\dot{P}$ is 1.99×10^{-20}, only one third of the measured value of 5.72×10^{-20} after correcting for the "train whistle" effect (e.g., Camillo, Thorsett, & Kulkarni 1995), the kinematic contribution to the measured $\dot{P}$ from the pulsar's transverse velocity of 92 km s^{-1}. Interestingly, this effect also limits the distance to PSR J0437–4715 to an absolute maximum of 215 pc. Its characteristic age is 4.6×10^9 yr, 6 times longer than the original estimate (Johnston et al. 1993), and consistent with estimates of the age of its white dwarf companion. Furthermore, its spin-down power, $I\Omega\dot{\Omega}$, is only 4×10^{33} ergs s^{-1}, almost an order of magnitude smaller than first reported, and less than that of the lowest luminosity γ-ray pulsars by the same factor.

The nature of the soft X-ray emission from PSR J0437–4715 is still not clear. Becker & Trümper (1993) suggested that, in addition to the mostly power-law spectrum, a blackbody component of temperature $T \sim 1.7 \times 10^6$ K and emitting area 0.05 km^2 might be be present that they associated with a peak at 0.9 keV in the pulsed fraction as a function of energy. Such a component would, of course, demand the operation of some mechanism of surface reheating; in all calculations neutron stars cool below 10^5 K after 10^6 yr. Estimates of the magnetic dipole and viewing geometry, albeit uncertain ones, were made by Manchester & Johnston (1995) using the rotating vector model of the radio polarization, which can aid in the interpretation of the X-ray pulse profile.

In this paper, we report the results of a long *EUVE* observation of PSR J0437–4715, together with a reanalysis of the *ROSAT* PSPC observation of the same source. A previous, shorter *EUVE* observation of PSR J0437–4715 was reported by Edelstein, Foster, & Bowyer (1995), but those data were not taken in the high time resolution mode which is necessary to see the pulsations. Furthermore, combined analysis of the *EUVE* and *ROSAT* pulse profiles and spectra enable us to reassess the question of thermal vs. nonthermal X-ray emission, and to place formal limits on the properties of any thermal components that may be present.

2. *EUVE* OBSERVATIONS AND TIMING ANALYSIS

The pulsar J0437–4715 was observed by *EUVE* during a 20 day period between 1994 October 23 and November 12, during which a valid exposure time of 495,897 s was obtained in the Deep Survey (DS) instrument. Events occurring when the line of sight to the source passed less than 400 km above the Earth's limb were rejected. A total of 4370 counts above background were collected from the pulsar through the Lexan filter, as determined in a 73″ radius extraction aperture. After accounting for deadtime and "Primbsching," the effective exposure time is reduced to 449,034 s. The resulting corrected count rate of 0.00973 s^{-1} was used in all calculations that require an absolute flux. To maximize the signal-to-noise ratio in the pulsed light curve, we also extracted counts within a smaller aperture of the DS, a carefully placed circle of radius 43″ which contains 95% of the source counts in the asymmetric source profile. The resulting light curve contains an estimated 4163 source counts, and only 937 background events.

Data were taken simultaneously by the three spectrometers pointed at the source, but no significant detection of the pulsar was made in these. The spectrometer data will not be discussed further here.

An updated pulsar and binary orbit ephemeris, including an accurate position, were kindly supplied by J. F. Bell. Millisecond pulsars are extremely stable clocks, and the radio ephemeris is accurate to 5 μs for the entire three-year period since the discovery of the pulsar. We first transformed the time of arrival of each photon to Barycentric Dynamical Time (TDB) using a procedure based on the Princeton TEMPO code, supplemented with the additional corrections for the changing orbital position of the *EUVE* satellite. The photon times were then corrected for the orbital Doppler delay within the 5.74 d binary system. The resulting pulse profile is shown in Figure 1. Background has been subtracted, and two cycles are graphed to guide the eye. There is one broad pulse per cycle, although it is narrower than a sinusoid. The pulsed fraction, defined conventionally as the fraction of the total counts lying above the minimum of the light curve, is 0.27 ± 0.05. The peak-to-trough ratio is approximately 1.8.

It is important to understand the possible sources of systematic error in the pulse profile in terms of the various effects that limit the accuracy of the final timing solution. A measurement of the pulse shape of this 5.75 ms pulsar is possible only because the observation was made in "WSZ" mode, which tags each photon with the full 0.5 ms time resolution of the the spacecraft clock. Although the spacecraft clock drifts at an average rate of $\sim 1 \times 10^{-8}$, the times in the data stream are kept to within ± 0.3 ms of UTC by the following procedure. Each time the clock drifts to +0.3 ms, a jump of –0.6 ms is applied to the data. This correction is applied on average 3.2 times per day. During the span of our observation, 61 such corrections were applied. By interpolating between these known discontinuities, we reduced this particular source of error to ~ 0.1 ms, resulting in a slightly sharper pulse profile. Another requirement for limiting systematic errors to 0.1 ms is knowledge of the satellite ephemeris to an accuracy of 30 km along its orbit. This condition has not been verified to our knowledge, but the design specification of 10 km is well within our requirements. Since the time resolution is still no better than 0.5 ms, fine details in the pulse profile may not be significant. In particular, the 20 bin light curve in Figure 1 oversamples the true time resolution by a factor of 2.

Even though we believe that the *relative* stability of the spacecraft clock was maintained to better than 0.5 ms over the 20 day span of the observation, the details of the pulse profile could also be affected by errors in *absolute* timing, if there are any. We do not believe that there are any such gross effects. For example, the *EUVE* data can itself be used to time the periastron passage of the pulsar, and it agrees with the radio ephemeris to within ± 15 s. Any errors in absolute time that are smaller than this would have a negligible effect on our results.

In deriving the pulse profile in Figure 1, it is important that we deliberately *did not* search over a range of pulsar and binary parameters, since the radio ephemeris is extremely accurate for our purposes. Unlike the radio, the X-ray pulse does not have a strong, narrow feature that can be used to optimize the ephemeris. Such a search would simply introduce large, spurious features into the pulse profile. In summary, we believe that the light curve in Figure 1 is grossly accurate in terms of pulsed fraction and non-sinusoidal shape, but that the individual bin-to-bin variations are not reliable. In particular, it is not clear if the top of the light curve is flat, cusped, or round.

3. *ROSAT* OBSERVATIONS AND TIMING ANALYSIS

The *ROSAT* PSPC observation of PSR J0437–4715 was originally reported by Becker & Trümper (1993). We have reanalyzed this observation in order to make joint spectral fits of the *ROSAT* and *EUVE* data for this presumably steady source, and to compare the pulse profile with the one from *EUVE*. A total exposure of 6142 s was obtained during three satellite orbits on 1992 September 20 and 21. Extraction of the source counts is relatively straightforward, except that at energies below 0.15 keV the electronic "ghost imaging" can smear the photon positions by as much as $2'.5$ from the centroid position. This particular observation is problematic because of the presence of a brighter soft X-ray source $4'.3$ from the pulsar, the former being the target of the observation in which the pulsar appeared serendipitously. As a compromise which extracted virtually all of the counts from the pulsar with negligible contamination from the neighboring source, we used a $1'.75$ extraction radius, and obtained a background measurement from a source-free circle with 4 times larger area, but located at a similar off-axis angle. The derived background is less than 5% of the source counts at all energies. The off-axis vignetting correction at this position for all energies

of interest is less than 2%, and was neglected. A net total of 1254 photons were detected in the 0.08–2.0 keV band, for an average count rate of 0.20 s^{-1}. There is no detection above 2.0 keV. A 3% correction for deadtime was applied in all calculations that require absolute fluxes.

Although the time resolution of the PSPC data is $\sim 130\mu s$, timing analysis of a millisecond pulsar is more problematic with *ROSAT* than with *EUVE*. The drift rate of the *ROSAT* spacecraft clock is $\sim 8 \times 10^{-8}$, an order of magnitude larger that that of *EUVE*, yet it was calibrated only once per week on average, as opposed to three times per day for *EUVE*. Inspection of the calibration data (e.g., Predehl 1994) reveals that nonlinearities in the drift rate cause residual errors of up to 2 ms per week that cannot be removed by fitting low-order functions to the calibration points. Furthermore, it is not clear that the day-to-day predictability of the spacecraft clock is much better than 1 ms.

Of the three spacecraft orbits that constitute the *ROSAT* observation of PSR J0437–4715, two are adjacent, but one came exactly 1 day (15 orbits) earlier. After performing the barycentric correction using the spacecraft clock calibrations contained in the PROS version 2.3.1 software, we folded the pulsar data separately for the three spacecraft orbits. Not surprisingly, the two adjacent orbits show pulse profiles which agree in phase, while the orbit separated by one day has a statistically significant phase offset of approximately 0.5 ms. Since the magnitude of this offset is typical of what is expected for clock drift, we interpreted it as such, and shifted the first orbit's data by 0.5 ms before coadding to make the final pulse profile shown in Figure 2. Subsequent details of our analysis are not significantly affected by this somewhat arbitrary procedure.

Our pulse profile is similar to that found by Becker & Trümper (1993). They found that the pulsed fraction is a strong function of energy, with an average of 0.30 ± 0.03 over the full *ROSAT* energy range, and a peak of 0.53 ± 0.06 in the 0.6–1.1 keV band. We find a slightly weaker dependence. The average pulsed fraction is 0.32 ± 0.05, and the sub-intervals illustrated in Figure 2 have pulsed fractions of 0.35 ± 0.04, 0.47 ± 0.09, and 0.19 ± 0.10, respectively, in the 0.08–0.53, 0.53–1.10, and 1.10–2.00 keV bands. The *EUVE* pulsed fraction of 0.27 ± 0.05 is not significantly different from the value of 0.30 ± 0.10 that can be measured from the smaller number of photons in the overlapping *ROSAT* band (0.08–0.20 keV). The error bars are dominated by the uncertainty in establishing the minimum in the light curve, and are estimated by eye. In summary, we have at most weak evidence for an increase in pulsed fraction from 0.27 at 0.1 keV to 0.47 at 1 keV. Above 1 keV, the statistics are too poor to determine a pulsed fraction.

The slight differences between our results can largely be explained by methodology. Becker & Trümper (1993) fitted sinusoids, while we used the more standard definition (counts above minimum) which is less dependent upon pulse shape. In any case, the evidence for an energy-dependent pulsed fraction is not as strong as the peak in Figure 2 of Becker & Trümper (1993) might lead one to believe, because the adjacent points in that figure are not independent, and because the peak is narrower than the resolution of the detector. It is also possible that their results differ from ours because they varied the longitude of periastron in their pulsar search to optimize some measure of the "best" fit. As we have argued above, such a procedure is not warranted, and could introduce spurious features into the pulse profile. If the pulse *shape* differs with energy, this would be a reason to reassess both of our methods of determining the pulsed fraction, and the meaning of the results. But as pointed out by Becker & Trümper (1993), there is no strong evidence for energy dependence in the pulse shape or phase. In summary we believe that there could be a weak dependence of pulsed fraction on energy. Our enthusiasm for fitting more than one component to the spectrum is somewhat dampened, but not completely drowned (see §4.2).

Since we are not yet confident about the *absolute* timing of the *ROSAT* data at the 1 ms level (or the *EUVE* data, for that matter), we do not attempt here to align the pulses in absolute phase with each other, or with the radio pulse.

4. COMBINED SPECTRAL ANALYSIS

There are likely pitfalls in fitting the *EUVE* and *ROSAT* data jointly because the nature of the error bars are completely different. The DS flux constitutes a single data point with very high statistical accuracy, but potentially disastrous systematics. The *ROSAT* error bars, on the other hand, are dominated by counting statistics. Therefore, we have chosen to apply a method in which

the *ROSAT* spectrum is first fitted over a generous grid of parameters, and then each of these trial spectra are folded thorough the DS effective are curve in order to find those models which are consistent with both instruments' data. In this way, the qualitatively different contribution of each to the errors can be seen. Only energies between 0.11 keV and 2.00 keV are included in the *ROSAT* spectral fits, corresponding to channels 3–30 in the standard 34 channel binning scheme. The 1993 January 12 response matrix was used. In all the Figures, channels 2–30 are displayed, but the channel 2 is not used in the fit. For the DS, the effective area curve used is that displayed in the Second *EUVE* Source Catalog (Bowyer et al. 1995).

4.1. *Single-Component Models*

As found by Becker & Trümper (1993), a single blackbody model gives an unacceptable fit to the *ROSAT* data, with $\chi^2 = 80$ for 25 degrees of freedom, $T = 1.5 \times 10^6$ K, and $N_{\rm H} = 0$. A simple power law gives an adequate fit, with $\chi^2 = 19.6$. Both fits are shown in Figure 3. The 90% confidence contour for the parameters of the power-law fit is shown in Figure 4. The best fitted column density of 9×10^{19} cm^{-2} is consistent with the dispersion measure of 2.65 cm^{-3} pc and a hydrogen ionization fraction of 0.1. The energy spectral index $\alpha = 1.45 \pm 0.25$ is consistent with the value of 1.6 ± 0.2 found by Becker & Trümper (1993), but our intrinsic luminosity of 5.0×10^{30} ergs s^{-1} in the 0.1–2.4 keV band ($d = 140$ pc) is about 17% less than theirs.

The fact that the target of this *ROSAT* observation was actually a soft X-ray-selected Seyfert galaxy from the *ROSAT* All-Sky Survey (RX J0437.4–4711), affords a serendipitous measurement of the total Galactic X-ray absorption on a line of sight only 4'.3 from PSR J0437–4715. A power law fitted the spectrum of this bright Seyfert very well, with $\chi^2_\nu = 0.905$, $f_{\rm x} = 1.47 \times 10^{-11}$ ergs cm^{-2} s^{-1}, $\alpha = 1.56 \pm 0.09$, and $N_{\rm H} = (1.01 \pm 0.16) \times 10^{20}$ cm^{-2}. We consider this value of $N_{\rm H}$ to be a reliable upper limit on the X-ray absorption to the pulsar, subject only to the caveat that $N_{\rm H}$ might be larger if there is really an unmodelled upturn in the soft X-ray spectrum of the Seyfert that makes it steeper than the fitted power law. For this source, we do not attempt a joint fit to the *EUVE* and *ROSAT* data taken 2 years apart because Seyfert galaxies are notoriously variable, especially those with very soft spectra. Such a comparison would likely be meaningless. Instead, a detailed analysis of the long *EUVE* light curve of this Seyfert galaxy is reserved for a later paper. We also note that RX J0437.4–4711 should be identified with EUVE J0437–471 as listed in the Second *EUVE* Source Catalog (Bowyer et al. 1995), and with the *Einstein* Slew Survey source 1ES 0435–472 (Elvis et al. 1992), whose position is consistent with that of the *ROSAT* source.

In order to test whether or not the *EUVE* flux of PSR J0437–4715 is consistent with the power-law fit to the *ROSAT* spectrum, we folded each of the trial *ROSAT* spectra corresponding to the fixed grid of Figure 4 through the effective area curve of the DS. The normalization constant for each trial was individually calculated from the total *ROSAT* counts. In this way, a grid of predicted DS counts was derived for comparison with the observed number. The range of spectral parameters acceptable to the DS is approximated by assigning a ±15% uncertainty to the predicted DS count rate to account for any relative errors in normalization between the effective areas of the two instruments. The resulting band of spectral parameters allowed by the DS overlaps the *ROSAT* confidence contour in Figure 4, implying that a single power law fits both instruments.

The principal contribution of the *EUVE* point is to restrict $N_{\rm H}$ to the lower end of the *ROSAT* range, namely $(5 - 8) \times 10^{19}$ cm^{-2}. This is consistent with what we know about the total column density in this direction from the adjacent Seyfert galaxy, which has $N_{\rm H} = (1.01 \pm 0.16) \times 10^{20}$ cm^{-2}, and with the dispersion measure that indicates an ionized column of $N_{\rm e} \sim 8 \times 10^{18}$ cm^{-2} toward the pulsar. At a Galactic latitude of −42°, the 140 pc line of sight to the pulsar passes through a neutral gas column about half that to infinity. Thus, the measured range of $(5 - 8) \times 10^{19}$ cm^{-2} is within expected limits.

Although the DS Lexan band is sensitive in the range 65–200 Å, photons are detected from PSR J0437–4715 only at the short wavelength end because of the steep increase in interstellar absorption as a function of wavelength. Figure 5 shows the effective distribution of detected counts from PSR J0437–4715 in the DS corresponding to the range of power-law models that fitted, with their correct normalizations, both the *ROSAT* and DS fluxes. Since nearly all the detected flux is at wavelengths shortward of 120 Å, we refer to this band conventionally as soft X-rays.

Our result contradicts the claim of Edelstein *et al.* (1995) that their earlier *EUVE* observation is inconsistent with a power-law fit to the *ROSAT* data unless the column density is as high as 2.5×10^{20} cm^{-2}, an unacceptably large value. We can only speculate that their conclusion was based on the use of the slightly more luminous and steeper power law reported by Becker & Trümper (1993), without regard to the *range* of individual normalizations that would be associated with a grid of acceptable fits. Our own power-law folds though both instruments are consistent with $N_{\rm H} = (5-8)\times10^{19}$ cm^{-2}.

Given the acceptable fit of a single power law with reasonable column density to both the *EUVE* and *ROSAT* data, and the lack of evidence for a blackbody component, one would be tempted to call a halt to the spectral fitting at this point. In fact, the $\chi^2_{\rm min}$ of the power-law model is almost *too* small. The probability of χ^2 exceeding the observed value of 19.6 is 77%. Therefore, the statistical quality of the data may not be good enough to support tests for deviations from a power law. Nevertheless, there are weak observational reasons, and strong theoretical reasons, to examine what contribution a blackbody component *might* make to the soft X-ray flux without violating observed limits. The observational reasons are the possible variation in pulsed fraction as a function of energy, and the fact that the peaks are not so strong and sharp as to rule out a contribution of a hot surface to either the pulsed or the unpulsed flux. The theoretical reason has do with estimates of polar cap heating from the impact of particles accelerated in the pulsar magnetosphere that predict thermal luminosities which are not insignificant compared to the observed X-ray luminosity of PSR J0437–4715. That some younger pulsars seem to display such components is also a motivation to examine such a scenario. Accordingly, we analyze two-component models in the following sections, one involving a power law plus blackbody, and the other a pair of blackbodies.

4.2. *Power Law plus Blackbody Model*

Becker & Trümper (1993) argued that a spectral decomposition in which a blackbody made a significant contribution to the flux between 0.6 and 1 keV was acceptable, and was motivated by the increase in pulsed fraction at these energies. Although we think that the evidence for an energy-dependent pulsed fraction is not so definitive, we nevertheless explore the possible range of power law plus blackbody fits to the spectrum. The model spectrum takes the form

$$F(E) = C\left(\frac{E^3}{e^{E/kT}-1} + f\,E^{-\alpha}\right)e^{-\sigma(E)N_{\rm H}}\ \ {\rm keV\,cm^{-2}\,s^{-1}\,keV^{-1}}. \qquad (1)$$

The method that we use in exploring the parameter space of this model is the same as that described in Halpern & Ruderman (1993) for the Geminga pulsar. Briefly, a full four-dimensional χ^2 grid is searched for acceptable values of the temperature T, energy spectral index α, column density $N_{\rm H}$, and power-law fraction f. For each trial spectrum, the overall normalization constant C is that which matches the total counts. Confidence limits can then be found by projecting the χ^2 grid onto any lower dimensional surface of interest.

The best such model is shown in Figure 6, and the 90% confidence contour for the blackbody component in the $(T, N_{\rm H})$ plane is shown in Figure 7. The decrease in $\chi^2_{\rm min}$ from 19.6 (in the power-law fit) to 12.8 justifies the addition of two parameters at the 99% level, according to the F test. However, this $\chi^2_{\rm min}$ is probably *too* small, as discussed above. The probability of χ^2 exceeding 12.8 is 95.6%. A column density less than 10^{19} cm^{-2} is formally possible in this model because the blackbody has an intrinsic downturn at low energy. Such a low value is conceivable if most of the interstellar medium in the line of sight is in the hot phase, a possibility which is not contradicted by any measurement that we are aware of.

If we adopt the dispersion-measure distance of 140 pc, then each trial fit can be translated to a surface area for the blackbody component. Because the fitted temperatures are relatively large, $T = (1.0-3.3)\times10^6$ K, the corresponding surface areas are quite small. The radius of the inferred hot spot ranges from 50–600 m, as indicated by the dashed contours in Figure 7, and its bolometric luminosity is $\sim 8.4\times10^{29}$ ergs s^{-1}. In comparison, the standard radius of the open field-line polar cap, $r_{\rm p} = (R\Omega/c)^{1/2}R$, is 1.9 km. Note that these area estimates are uncertain by a factor of a few because of the time-averaged projection effects that depend on the unknown viewing geometry of the assumed small, hot region. We also neglect the possible deviations of

realistic model atmospheres from a blackbody, which tend to lower the temperatures that can fit a given observed spectrum (Romani 1987; Miller 1992). The results of this model are similar to those of Becker & Trümper (1993), who found a temperature of $\sim 1.7 \times 10^6$ K and an emitting area of 0.05 km^2 ($r \sim 125$ m). But Figure 7 shows the full range of parameters allowed by this fit. In view of the weak need for a thermal component to begin with, the areas could be interpreted as upper limits rather than estimates.

Finally, we superpose a contour that corresponds to agreement with the observed *EUVE* DS flux. As before, the main contribution of the DS measurement is to restrict the column density to less than 8×10^{19} cm^{-2}. It is important to realize that, in this model, it is still the power law that makes the dominant contribution to the *EUVE* detection. Figure 6 shows that the thermal component contributes less than 10% of the flux below 0.2 keV. At 0.7 keV, however, the thermal contribution is about 40% of the total, which could be consistent with the slight increase in pulsed fraction at that energy (47% as opposed to $\sim$ 32% on average). This scenario would require the thermal component to be more highly pulsed than the power law, and nevertheless have the same phase. In §5.2, we consider the related hypothesis that some of the steady, power-law X-ray flux might originate in the bow shock.

4.3. *Double Blackbody Model*

It is possible for both the *EUVE* flux and "soft" *ROSAT* band to be dominated by blackbody emission, but only if the "hard" *ROSAT* flux is a separate blackbody component, and not a power law. Following the same method as in the previous section, we searched a four-dimensional parameter space of two temperatures, T_1 and T_2, column density $N_{\rm H}$, and fraction f which is closely related to the ratio of surface areas A_2/A_1 of the two blackbody components. The form of the model spectrum is

$$F(E) = C\,E^3 \left(\frac{1}{e^{E/kT_1} - 1} + \frac{f}{e^{E/kT_2} - 1} \right) e^{-\sigma(E) N_{\rm H}} \ \ {\rm keV\,cm^{-2}\,s^{-1}\,keV^{-1}}. \qquad (2)$$

Figure 8 is an example of the best such fit, and Figure 9 shows the allowed spectral parameters for the *softer* blackbody ($T_1, N_{\rm H}$). The decrease in $\chi^2_{\rm min}$ from 19.6 in the power-law fit to 14.5 justifies the addition of two parameters at the 97% level, according to the F test. As before, contours of surface area A_1 for the softer blackbody are superposed as dashed lines in Figure 9. The ratio of areas A_2/A_1 (not shown) ranges from $10^{-4} - 10^{-2}$ in all cases.

The effect of the *EUVE* point is, as before, to restrict the column density to less than 8×10^{19} cm^{-2}. The overlap between the *EUVE* and *ROSAT* contours restricts the soft blackbody parameters to the range $4 \times 10^5 < T_1 < 12 \times 10^5$ K, and $2 < A_1 < 200$ km^2. Thus, the upper limit on the emitting area is less than 20% of the typical area of a neutron star, and may be comparable to that of the open field-line polar cap, ~ 11 km^2 for this rotation period.

In this model the softer blackbody component dominates the *EUVE* DS flux and *ROSAT* PSPC carbon band with a bolometric luminosity of $L_1 \sim 1.8 \times 10^{30}$ ergs s^{-1}, while the harder component with $L_2 \sim 1.5 \times 10^{30}$ ergs s^{-1} dominates the PSPC spectrum above 0.5 keV. This is an important distinction from the previous model, in which the power-law component makes the major contribution across the entire observed band. While the double blackbody model dispenses with the power-law component entirely, it leaves us with the question of why two thermal components that differ in area by several orders of magnitude should produce pulse profiles that are so similar. However, as long as both areas are concentric and much smaller than the neutron star, the resulting pulse shapes are expected to be the same. Alternatively, nature might be more realistic by employing a continuous range of temperatures in a way that produces a roughly energy-independent pulse shape. Finally, we remind the reader (and ourselves) that we embarked upon an investigation of these two-component models only to develop upper limits on thermal components. Perhaps they don't exist at all.

5. INTERPRETATION

5.1. *Pulse Profile and Dipole Geometry*

Possible interpretations of the X-ray pulse profile include hot spots at the magnetic polar caps, and beaming of nonthermal radiation along the open magnetic field lines. Quite specific information about the magnetic geometry and viewing direction of pulsars can be derived from the rotating vector model of the radio polarization, which often represents the sweep of position angle with phase very well. In the case of PSR J0437–4715, there is significant radio emission over at least 80% of the pulse period, but the complex details of the position angle variations are not fitted well by the simple model (Manchester & Johnston 1995). Deviations are not unexpected from millisecond pulsars, since the emission region is likely to be close enough to the surface for higher order multipoles of the magnetic field to have a significant effect on the polarization. Although the pulse profile is itself complex, Manchester & Johnston concluded that the strong "core" component indicates that the magnetic axis crosses close to our line of sight. Despite possible complicating details, they conclude that the overall shape of the position angle variation favors magnetic inclination angle $\alpha = 145°$, and viewing angle $\zeta = 140°$, both measured from the rotation axis. In this geometry, and for a dipole centered on the star, the opposite magnetic pole remains more than 15° below the limb at all times, which is consistent with the absence of an interpulse in the radio, and in the X-ray if the latter is at least moderately beamed.

This geometry does not clearly distinguish between thermal and nonthermal models for the X-ray pulse for two reasons. First, thermal emission from the opposite polar cap may still be visible because of strong light bending at the surface of the neutron star. Indeed, such an effect may be responsible for some of the substantial X-ray emission seen at pulse minimum. Detailed modelling of the light bending effect in this specific geometry for various assumed values of M/R would be necessary to determine whether the observed pulse profile is consistent with thermal emission from both poles. Second, the simple centered dipole may not be a correct description of the *surface* magnetic field geometry, even to a first approximation. Indeed, there are theoretical reasons to think that this is the case for millisecond pulsars (Chen & Ruderman 1993), and observations of thermal X-ray components in ordinary pulsars always show only one pulse per rotation period (e.g., Halpern & Ruderman 1993). As mentioned earlier, the coincidence of the X-ray phase at all energies is problematic for models in which both thermal and nonthermal processes contribute. Time of flight delays and differential relativistic aberration between the pulsar's surface and magnetosphere are substantial. Ultimately, the absolute time of arrival of the X-ray pulse with respect to the radio will reveal important information about the relative heights of the radio and X-ray emitting regions, but this analysis is not yet reliable at the ms level. For these reasons, we must rely on the X-ray spectrum for additional clues about the sources of emission.

5.2. Sources of Nonthermal Emission

If most of the soft X-ray emission from PSR J0437–4715 is to be described as a nonthermal power law, then it must flatten in the far ultraviolet so as not to exceed the observed brightness of the $B = 22$ optical companion (Bell et al. 1993; Danziger et al. 1993). The X-ray power law of slope 1.45 would extrapolate to $B = 16.7$. A power law connecting the actual blue flux to the observed X-ray flux at 200 eV would have a spectral index of 0.30. The real ultraviolet spectrum must therefore be flatter on average than 0.3. The X-ray and assumed far UV spectrum could be synchrotron radiation in the $< 3.4 \times 10^8$ G magnetic field near the surface of the neutron star, as the cyclotron frequency eB/mc falls in the visible band. Electrons with Lorentz factor $\gamma \gtrsim 10$ would produce the soft X-rays that we see. Alternatively, synchrotron emission from the outer magnetosphere, within the light cylinder of radius $r_{lc} = 2.7 \times 10^7$ cm, could involve electrons of $\gamma \gtrsim 2000$ and $B \sim 10^4$ G. Our default interpretation is that most of the X-ray flux from PSR J0437–4715 is magnetospheric in origin, similar to that of ordinary, young pulsars, with the rather low pulsed fraction perhaps resulting from a broader beaming pattern related to the large opening angle of the open field-line region expected for millisecond pulsars, and observed in the radio.

The observed flux and its plausible extrapolations to low and high energies account for a negligible fraction of the spin-down power of the pulsar, $I\Omega\dot{\Omega} = 4 \times 10^{33}$ ergs s^{-1}. The *SIGMA* telescope aboard the *GRANAT* spacecraft derived an upper limit of 7×10^{32} ergs s^{-1} in the 40–200 keV range (Barret et al. 1994), which is not very restrictive. More significantly, an upper limit of 1.7×10^{32} ergs s^{-1} above 100 MeV can be deduced from the first 2 1/2 years of EGRET data (Fierro et al. 1995; Thompson et al. 1995), which means that PSR J0437–4715 is a significantly

less efficient high-energy γ-ray emitter than the middle-aged pulsars Geminga and PSR B1055–52. Leaving aside the possible importance of beaming geometry, it could be the case that, as speculated by Ruderman et al. (1993), pulsars channel an increasing fraction of their spin-down power into γ-ray luminosity until both approach $\sim 3 \times 10^{34}$ ergs s^{-1}, at which point the outer gap accelerator turns off. Since PSR J0437–4715 is an order of magnitude weaker in its spin-down power than Geminga and PSR B1055–52, both of which have $I\Omega\dot{\Omega} = 3 \times 10^{34}$ ergs s^{-1}, it may lie well to the wrong side of the outer-gap death line.

As is probably the case for most pulsars, the majority of the spin-down power is carried out in a wind of relativistic particles that ultimately deposits its energy in the interstellar medium. In the case of PSR J0437–4715, there is a direct quantitative measure of this process in the form of a bow-shock nebula (Bell et al. 1993; 1995) that points in the direction of the proper motion. We can use the usual argument that equates the ram pressure of the interstellar medium to the pulsar wind pressure at the apex of the bow shock to solve for the density of the ambient medium,

$$\rho_0 = \frac{I\Omega\dot{\Omega}}{4\pi\, r_{\rm w}^2\, v_{\rm p}^2\, c}. \tag{3}$$

Here $r_{\rm w}$ is the distance from the pulsar to the apex of the bow shock, and $v_{\rm p}$ is the velocity of the pulsar. Since lower limits to $r_{\rm w}$ and $v_{\rm p}$ are accurately known (projected values of 1.9×10^{16} cm and 92 km s^{-1}, respectively), an upper limit of 3.6×10^{-25} g cm^{-3} can be derived for ρ_0, corresponding to $n_{\rm H} \leq 0.15$ cm^{-3}. Since we do not imagine $n_{\rm H}$ to be much less than this upper limit, a large fraction of $I\Omega\dot{\Omega}$ must be dissipated by the shock.

The pulsar's velocity is too low to account for any of the unpulsed X-ray flux as post-shock thermal emission. But since the observed X-ray luminosity of PSR J0437–4715 is only $\sim 10^{-3} I\Omega\dot{\Omega}$, it is possible that some of the unpulsed X-ray flux might be synchrotron emission from relativistic electrons and positrons of $\gamma \sim 10^7$, radiating in the magnetic field of $\sim 2 \times 10^{-5}$ G that would be pulled out in equipartition with the wind from the light cylinder to the location of the shock. Particles can be accelerated to this energy because the maximum potential drop generated by the pulsar, $\Delta V_{\rm max} \sim (\Omega^2 B R^3)/(2c^2)$, is $\sim 6.7 \times 10^{13}$ V, corresponding to $\gamma \simeq 10^8$. This mechanism has been invoked to explain the weak X-ray flux from the only other millisecond pulsar to be detected in X-rays, PSR B1957+20 (Kulkarni et al. 1992). But since the X-ray luminosity in that case, $\sim 8 \times 10^{30}\, (d/1\,{\rm kpc})^2$ ergs s^{-1}, is only $\sim 10^{-4}$ of the spin-down power, PSR B1957+20 is perhaps not a precedent for expecting shock emission to contribute to the X-ray spectrum of PSR J0437–4715. Furthermore, the X-rays from PSR B1957+20 appeared not to be spatially extended in a *ROSAT* HRI image (Fruchter et al. 1992). Nevertheless, extended emission from the nebula at the analogous level of $\sim 4 \times 10^{29}$ ergs s^{-1} is certainly worth looking for in a long *ROSAT* HRI exposure of PSR J0437–4715.

5.3. Thermal Emission and Surface Reheating

The two-component models investigated here favor blackbody emission at temperatures of either $(4 - 12) \times 10^5$ K, or $(1.0 - 3.3) \times 10^6$ K, and from areas that are much smaller than the full surface of the neutron star. If these are taken as detections rather than upper limits, it would mean that thermal reheating is taking place, as neutron stars in all standard calculations cool below 10^5 K after 10^6 yr. A number of proposed thermal reheating mechanisms were evaluated by Edelstein et al. (1995) to account for the putative thermal component. These included 1) dissipation of internal heat generated by unpinning of vortex lines, 2) accretion from the interstellar medium, 3) accretion from the white-dwarf companion, 4) and nucleon decay catalyzed by magnetic monopoles. They found the first three of these to be inadequate, and we will not consider them further here, except to remark that their statement that "standard frictional heating models are virtually ruled out" is misleading. The heating rates produced by those models may be perfectly correct, but *additional* sources of heat may be necessary to account for the observed luminosity of PSR J0437–4715. A particular model can be proven defective only if predicts more heat than is observed, not if it predicts less.

The observation that the thermally emitting region must be comparable to or smaller than the open field-line polar cap, of radius $r_p = 1.9$ km, motivates us to consider another type of surface reheating, the bombardment of the polar cap region by energetic particles produced in the accelerators that are responsible for radio and high-energy emission. Direct evidence for such a process is seen in the X-ray emission from Geminga (Halpern & Ruderman 1993) and other intermediate-age pulsars (Finley 1994; Ögelman 1994), and especially from PSR B1929+10 (Yancopoulos, Hamilton, & Helfand 1994), a 3×10^6 yr old pulsar in which the 3×10^6 K blackbody emission comes from an area less than 50 m in radius. The same mechanism may also explain the weak X-ray flux from the 1.7×10^7 yr old pulsar PSR B0950+08 (Manning & Willmore 1994).

The maximum efficiency of heating by magnetospheric processes can be estimated following Halpern & Ruderman (1993). We multiply the Goldreich-Julian current density by the area of the polar caps to find an upper limit on the impacting particle flux,

$$\dot{N} < 2 \left(\frac{\Omega B}{2\pi e}\right) \left(\frac{\pi}{2}\frac{R\Omega}{c}\right) R^2 = 1.4 \times 10^{31} \text{ s}^{-1}. \quad (4)$$

The residual energy with which those particles impact the polar cap after radiating most of their energy via curvature radiation is,

$$E = \left[\frac{2e^2\,\Omega}{mc^3} \ln\left(\frac{r_{\rm in}}{R}\right)\right]^{-1/3} mc^2 \sim 2.3 \text{ ergs}, \quad (5)$$

Here, $r_{\rm in}$ is the inner radius of the accelerator region, which we take to be $\sim 10^7$ cm in this case. The maximum power brought down to the polar cap is then $L_p = \dot{N}E \leq 3.2 \times 10^{31}$ ergs s^{-1}.

This maximum heating rate is undoubtedly not operating because, if it were, the same accelerated particles would be radiating nearly the full spin-down power of PSR J0437–4715 in high-energy γ-rays. Rather, we suppose that the upper limit $L_\gamma < 1.7 \times 10^{32} = 0.04\, I\Omega\dot{\Omega}$ implies that either the size or the efficiency of the accelerator is less than 0.04 times the maximum value. Scaling the surface heating rate accordingly yields $L_p < 1.3 \times 10^{30}$ ergs s^{-1}. This is a comfortable value, for it can accommodate an interpretation of part of the observed X-ray luminosity as thermal without violating any of the upper limits. We conclude that even though the evidence for a thermal component is weak, a fraction of the observed X-ray luminosity could be understood as arising from the polar caps heated by particles accelerated in the magnetosphere without violating observational limits on γ-ray emission.

6. SUMMARY

The main purpose of this investigation was to examine the origin of the soft X-ray flux in the 5.75 ms pulsar J0437–4715. Plausible alternatives include magnetospheric synchrotron emission, surface thermal emission, and, for the unpulsed flux only, synchrotron emission at the pulsar wind's bow shock. Unfortunately, it is still not possible to rule out significant contributions from any of these mechanisms, as the light curve and spectrum do not strongly discriminate among them. The light curve in the *EUVE* DS (65–120 Å) consists of a single broad pulse containing $\sim 27\%$ of the flux, similar to that of the *ROSAT* data in the overlapping energy band. A combined analysis of the *EUVE* and *ROSAT* data is consistent with a power-law spectrum of intrinsic luminosity 5×10^{30} ergs s^{-1} in the 0.1–2.4 keV band, and $\alpha = 1.2 - 1.5$. The effect of the *EUVE* flux is to limit the column density $N_{\rm H}$ to the range $(5-8) \times 10^{19}$ cm^{-2}. For comparison, a nearby soft X-ray Seyfert galaxy determines the total Galactic column in this direction, $N_{\rm H} = 1 \times 10^{20}$ cm^{-2}.

When we apply two-component spectral fits to the combined *EUVE/ROSAT* data, we find that a small, hot polar cap of radius 50–600 m and temperature $(1.0-3.3) \times 10^6$ K could also be present. The principal motivation for including this component is a possible increase at ~ 0.9 keV in the pulsed fraction as a function of energy. The luminosity of such a region, $\sim 8 \times 10^{29}$ ergs s^{-1}, would most likely be powered by the impact of high-energy particles accelerated in the magnetosphere and flowing down along the open field lines. Alternatively, a larger region with $T_1 = (4 - 12) \times 10^5$ K

and $A_1 < 200$ km^2, might contribute the majority of the *EUVE* and soft X-ray flux, but only if a smaller, hotter component were present as well. Purely thermal models permit values of N_H as low as 10^{19} cm^{-2}.

We are not confident that the existence of a small, thermally emitting region will stand up to detailed modelling which takes into account the magnetic and viewing geometry inferred from the sweep of radio polarization angle. Whereas the modulation due to the thermal component would have to very large to cause an observable energy dependence, the actual modulation from a polar cap may be small because it remains more than 15° above the limb at all times, according to the results of the rotating vector model. This, plus the additional flux bent around the horizon from the opposite polar cap, may conspire to keep the pulsed fraction small. Of course, this potential difficulty could be sidestepped by abandoning the assumption of a simple centered dipole, and assigning the polar caps to arbitrary locations on the star.

One fact that does seem more understandable now than previously is the absence of high-energy γ-ray emission from PSR J0437–4715. Its kinematically corrected spin-down power is only 4×10^{33} ergs s^{-1}, which is an order of magnitude less than that of the lowest-luminosity γ-ray pulsars Geminga and PSR B1055–52. The absence of high-energy γ-rays from PSR J0437–4715 might signify an inefficient or dead outer gap accelerator. If any of the surface thermal X-ray emission from those efficient γ-ray pulsars is due to heating by particles streaming down from their accelerators, then the lack of a more luminous reheated surface on PSR J0437–4715 is not unexpected.

We thank Roger Romani for pointing out the discontinuity in the *ROSAT* timing of the observation of PSR J0437–4715, and David Helfand for helpful discussions and a critical reading of the manuscript. This work was supported by NASA grants NAG 5–1935 and NAG 5–2569. This paper is contribution No. 572 of the Columbia Astrophysics Laboratory.

REFERENCES

Bailyn, C. D. 1993, ApJ, 411, L83
Barret, D., et al. 1994, A&A, 288, 472
Becker, W., & Trümper, J. 1993, Nature, 365, 528
Bell, J. F. 1995, private communication
Bell, J. F., Bailes, M., & Bessell, M. S. 1993, Nature, 364, 603
Bell, J. F., Bailes, M., Manchester, R. N., Weisberg, J. M., & Lyne, A. G. 1995, ApJ, 440, L81
Bowyer, S., et al. 1995, ApJS, in press
Camillo, F., Thorsett, S. E., & Kulkarni, S. R. 1994, ApJ, 421, L15
Chen, K., & Ruderman, M. 1993, ApJ, 408, 179
Danziger, I. J., Baade, D., & Della Valle, M. 1993, A&A, 276, 382
Edelstein, J., Foster, R., & Bowyer, S. 1995, ApJ, in press
Elvis, M., Plummer, D., Schachter, J., & Fabbiano, G. 1992, ApJS, 80, 258
Fierro, J. M., et al. 1995, ApJ, 447, 807
Finley, J. P. 1994, in The Soft X-ray Cosmos, ed. E. M. Schlegel, & R. Petre (New York: AIP), 41
Fruchter, A. S., Bookbinder, J., Garcia, M. R., & Bailyn, C. D. 1992, Nature, 359, 303
Halpern, J. P. & Ruderman, M. 1993, ApJ, 415, 286
Johnston, S., et al. 1993, Nature, 361, 613
Kulkarni, S. R., Phinney, E. S., Evans, C. R., & Hasinger, G. 1992, Nature, 359, 300
Manchester, R. N., & Johnston, S. 1995, ApJ, 441, L65
Manning, R. A., & Willmore, A. P. 1994, MNRAS, 266, 635
Miller, M. C. 1992, MNRAS, 255, 129
Ögelman, H. 1994, in Lives of Neutron Stars, ed. M. A. Alpar et al. (Dordrecht: Kluwer), 101
Predehl, P. 1994, in The *ROSAT* Users' Handbook, ed. U. G. Briel et al. (Garching: Max-Planck-Institut), 59
Romani, R. W. 1987, ApJ, 313, 178
Ruderman, M., Chen, K., Cheng, K. S., & Halpern, J. P. 1993, in Proc. Compton Symposium, ed. M. Friedlander, N. Gehrels, & D. J. Macomb (New York: AIP), 259
Thompson, D. J., et al. 1995, ApJS, in press
Yancopoulos, S., Hamilton, T. T., & Helfand, D. J. 1994, ApJ, 429, 832

FIGURE CAPTIONS

FIG. 1.– Soft X-ray pulse profile of PSR J0437–4715 from the *EUVE* Deep Survey instrument. Background has been subtracted. The phase is arbitrary. Note that the time resolution is at best 0.5 ms, or 2 bins in the light curve. The data are repeated for two cycles to guide the eye. The pulsed fraction is 0.27 ± 0.05.

FIG. 2.– X-ray pulse profile of PSR J0437–4715 in the *ROSAT* PSPC. Background has been subtracted. The phase is arbitrary. The top panel shows all the data in the 0.08–2.0 keV range, and the lower three panels show the same data separated into three energy bands. Pulsed fractions are indicated at the lower left of each panel. The data are repeated for two cycles to guide the eye.

FIG. 3.– Fit of single-component models to the *ROSAT* PSPC spectrum of PSR J0437–4715. The lowest channel displayed was not used in the fit (a) Power-law fit with $\chi^2_\nu = 0.78$, $\alpha = 1.45$, $N_{\rm H} = 9 \times 10^{19}\,{\rm cm}^{-2}$, $L_{\rm X} = 5.0 \times 10^{30}$ ergs s^{-1}. (b) Blackbody fit with $\chi^2_\nu = 3.2$, $T = 1.5 \times 10^6$ K, $N_{\rm H} = 0$.

FIG. 4.– Confidence contours for the power-law fit. The 90% confidence level for the *ROSAT* PSPC spectrum corresponds to the case of two interesting parameters $(\alpha, N_{\rm H})$. The *EUVE* contour corresponds to agreement of the observed count rate in the DS to within ±15% of the value predicted by folding the corresponding *ROSAT* spectrum through the DS effective area curve. The shaded region indicates the spectral range jointly allowed by both instruments.

FIG. 5.– Effective distribution of counts in the *EUVE* DS corresponding to the range of spectral parameters allowed by the joint power-law fit (the shaded region in Figure 4). Integrals under the curves are within ±15% of the observed count rate.

FIG. 6.– Fit of the power law plus blackbody model to the X-ray spectrum of PSR J0437–4715. (a) Raw counts and model spectra folded through the detector response matrix. (b) Unfolded spectral model.

FIG. 7.– Confidence contours for the parameters of the blackbody X-ray component in the power law plus blackbody fit. The 90% confidence level for the *ROSAT* PSPC spectrum corresponds to the case of three interesting parameters $(T, N_{\rm H}, C)$. The contour marked *EUVE* corresponds to agreement of the observed count rate in the DS to within ±15% of the value predicted by folding the corresponding *ROSAT* spectrum through the DS effective area curve. The shaded region indicates the spectral range jointly allowed by both instruments. The dashed lines are the corresponding radii, in meters, of the emitting area at the assumed distance of 140 pc.

FIG. 8.– Fit of the double blackbody model to the X-ray spectrum of PSR J0437–4715. (a) Raw counts and model spectra folded through the detector response matrix. (b) Unfolded spectral model.

FIG. 9.– Confidence contours for the parameters of the softer blackbody X-ray component in the double blackbody fit. The 90% confidence level for the *ROSAT* PSPC spectrum corresponds to the case of three interesting parameters $(T_1, N_{\rm H}, C)$. The contour marked *EUVE* corresponds to agreement of the observed count rate in the DS to within ±15% of the value predicted by folding the corresponding *ROSAT* spectrum through the DS effective area curve. The shaded region indicates the spectral range jointly allowed by both instruments. The dashed lines are the corresponding contours of area A_1, in km^2, of the soft blackbody component at the assumed distance of 140 pc.

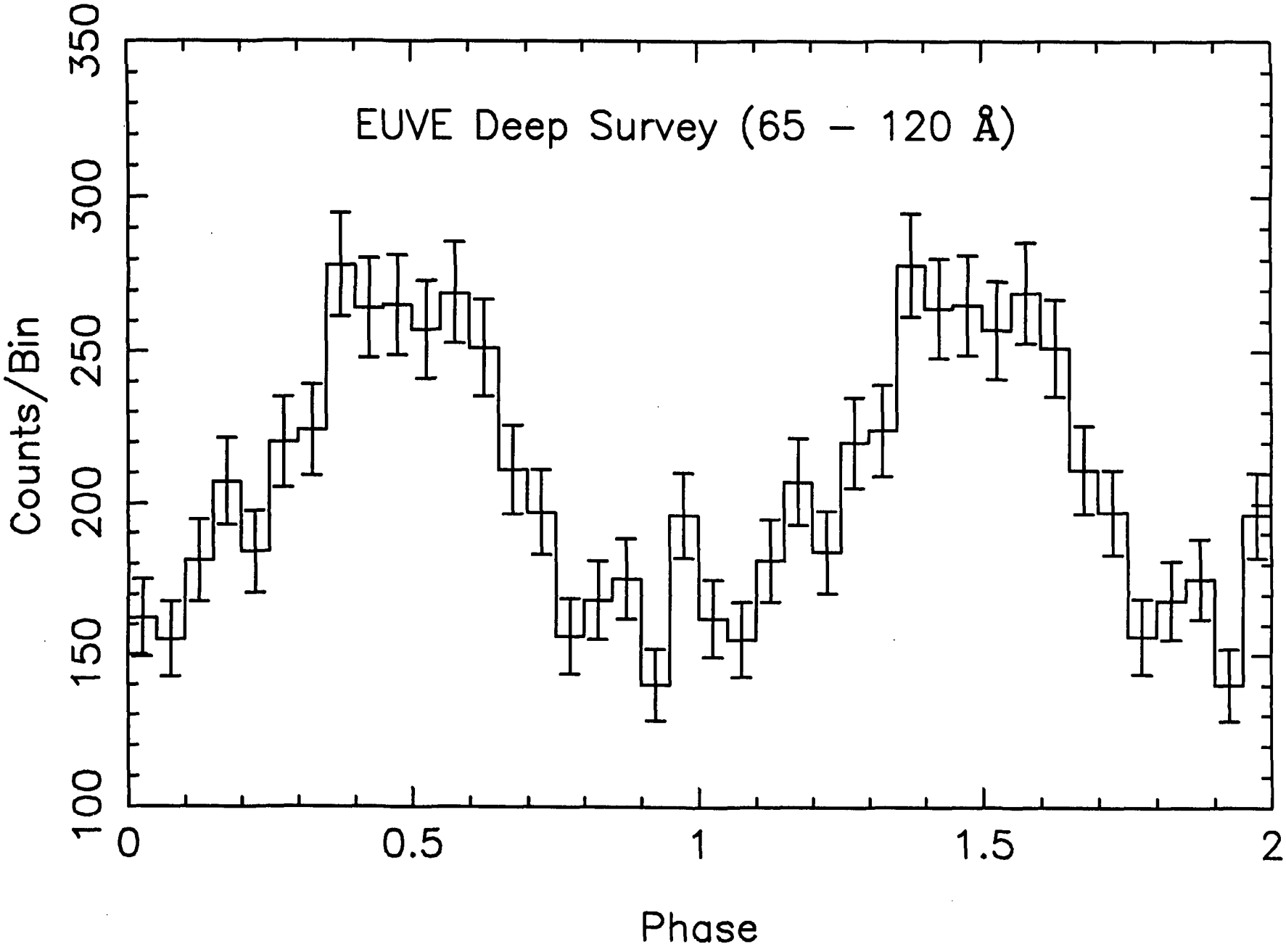
EUVE Deep Survey (65 – 120 Å)
Counts/Bin
100
150
200
250
300
350
0
0.5
1
1.5
2
Phase

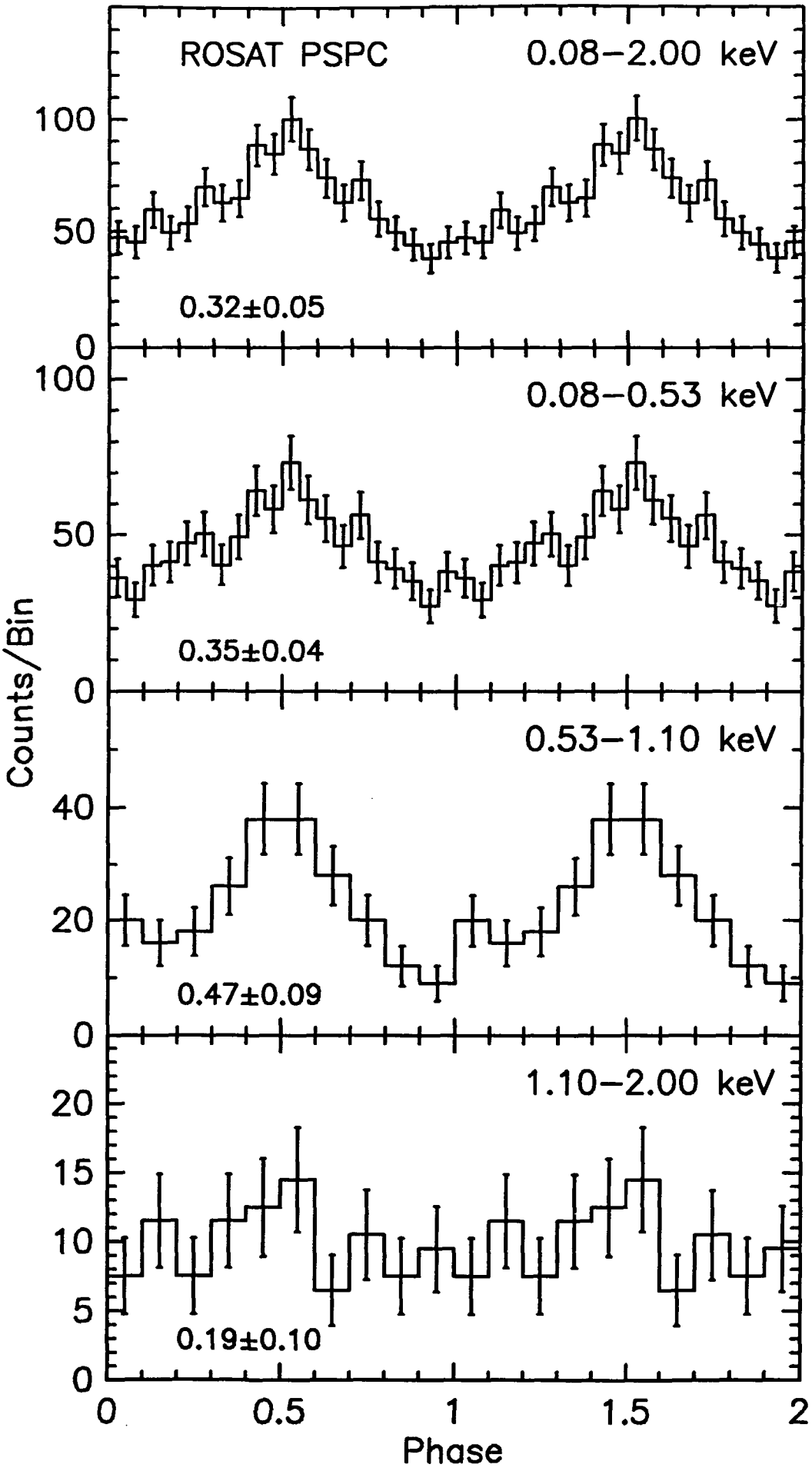
ROSAT PSPC
0.08–2.00 keV
0.32±0.05
0.08–0.53 keV
0.35±0.04
0.53–1.10 keV
0.47±0.09
1.10–2.00 keV
0.19±0.10
Counts/Bin
Phase

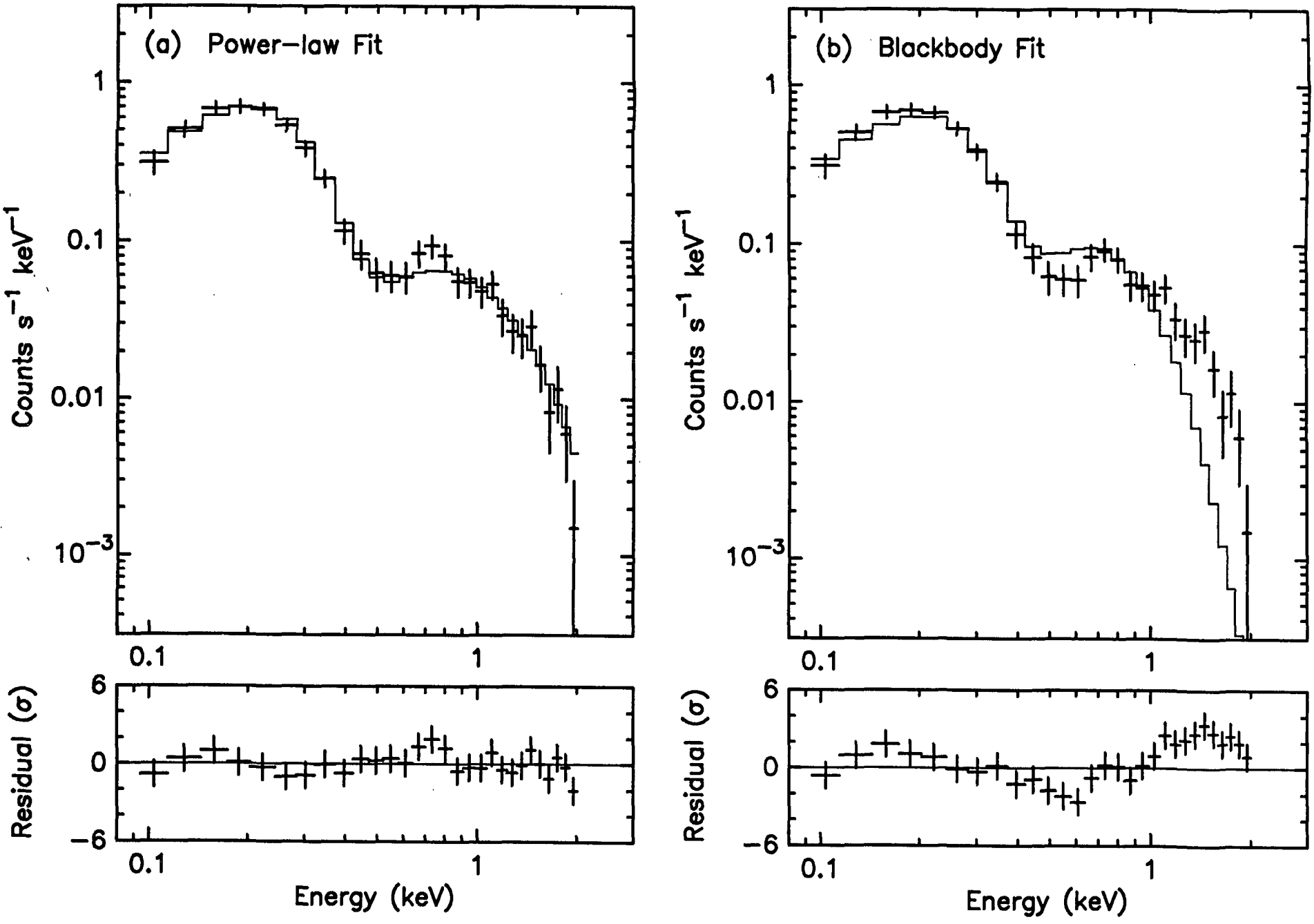
(a) Power-law Fit
(b) Blackbody Fit
Counts s^{-1} keV^{-1}
1
0.1
0.01
10^{-3}
Residual (σ)
6
0
−6
0.1
1
Energy (keV)

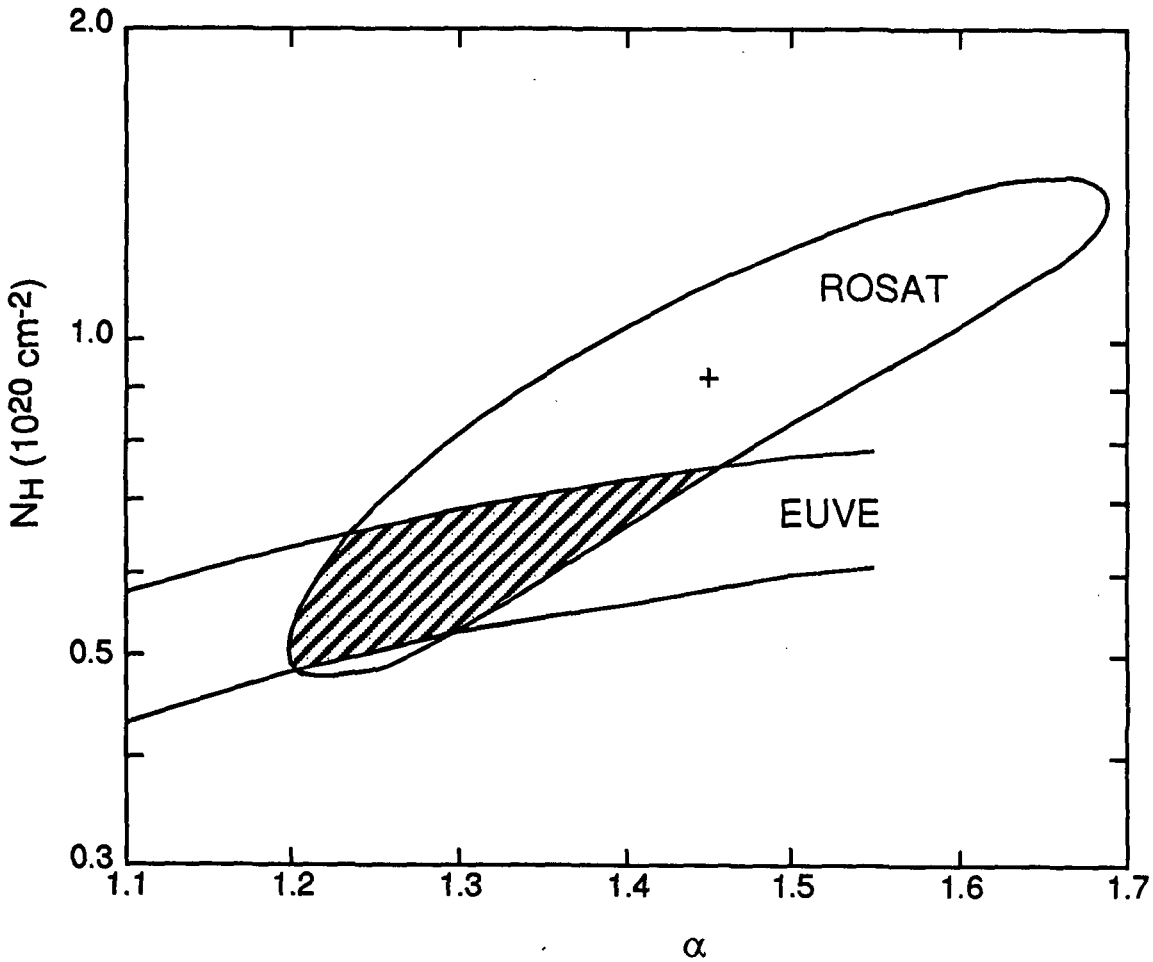
2.0
1.0
0.5
0.3
N_H (10^{20} cm^{-2})
ROSAT
EUVE
1.1
1.2
1.3
1.4
1.5
1.6
1.7
α

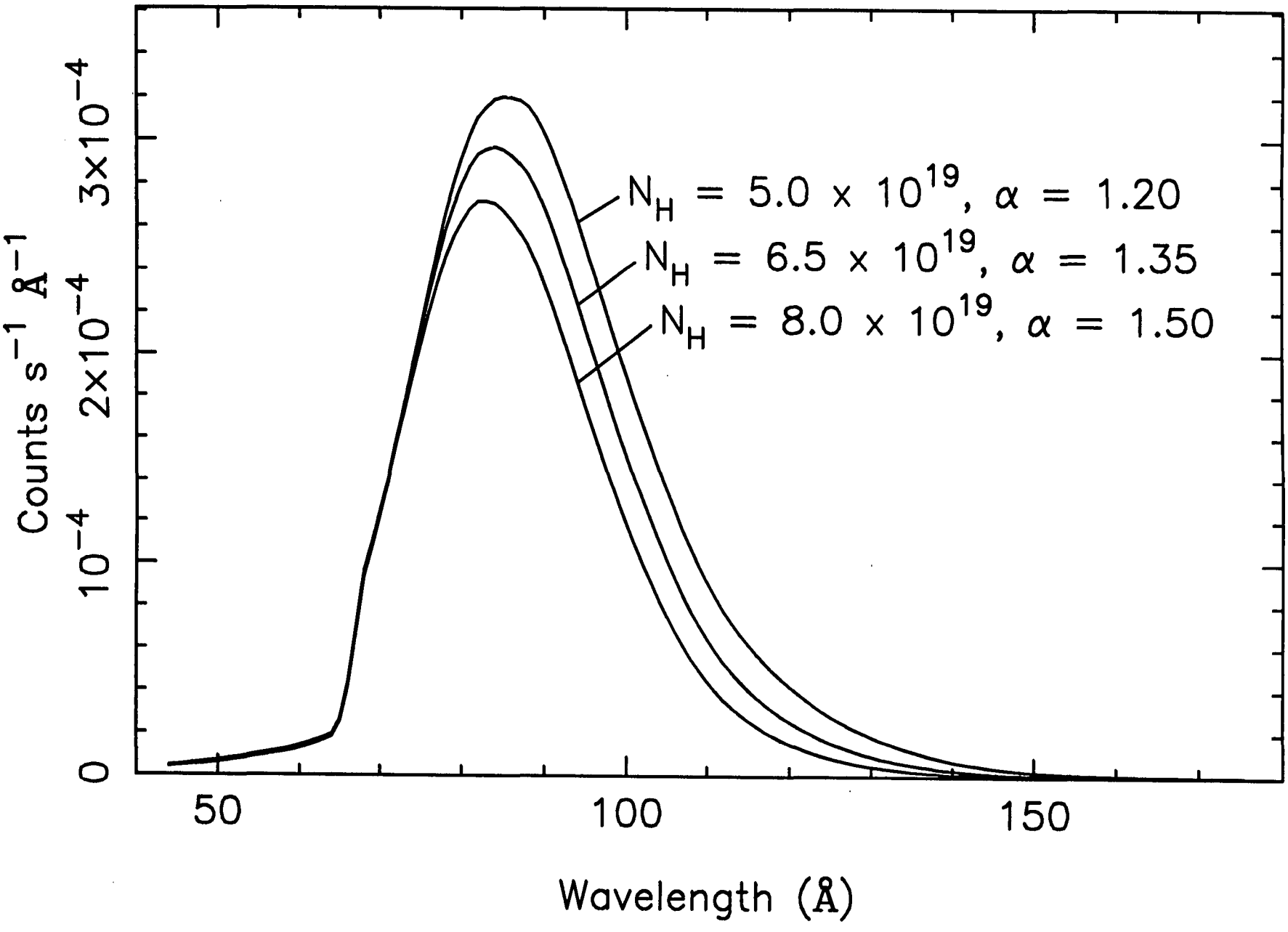
Counts s^{-1} Å^{-1}
0
10^{-4}
2×10^{-4}
3×10^{-4}
50
100
150
Wavelength (Å)
N_H = 5.0 x 10^{19}, α = 1.20
N_H = 6.5 x 10^{19}, α = 1.35
N_H = 8.0 x 10^{19}, α = 1.50

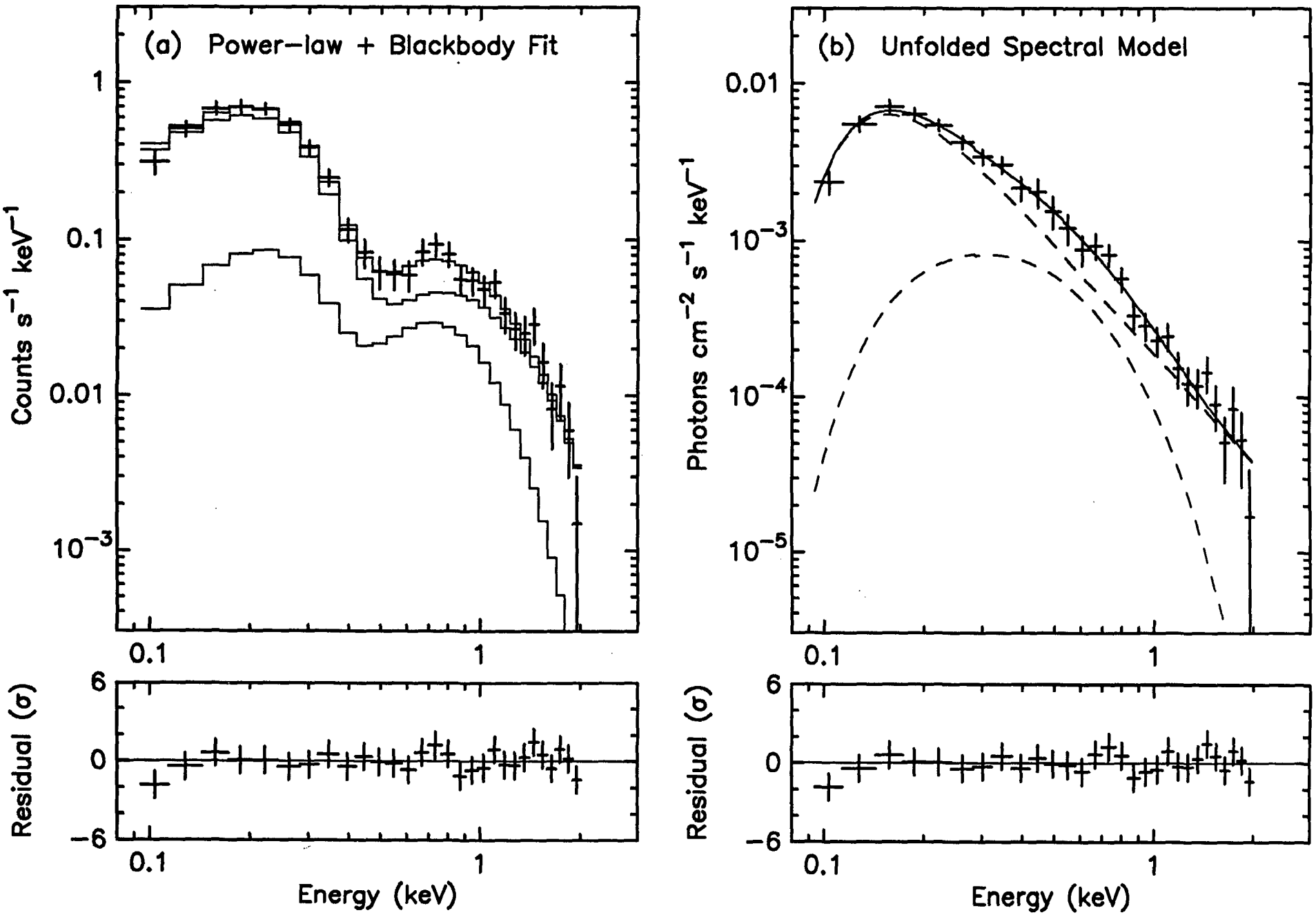
(a) Power–law + Blackbody Fit
Counts s^{-1} keV^{-1}
1
0.1
0.01
10^{-3}
0.1
1
Residual (σ)
6
0
−6
0.1
1
Energy (keV)
(b) Unfolded Spectral Model
Photons cm^{-2} s^{-1} keV^{-1}
0.01
10^{-3}
10^{-4}
10^{-5}
0.1
1
Residual (σ)
6
0
−6
0.1
1
Energy (keV)

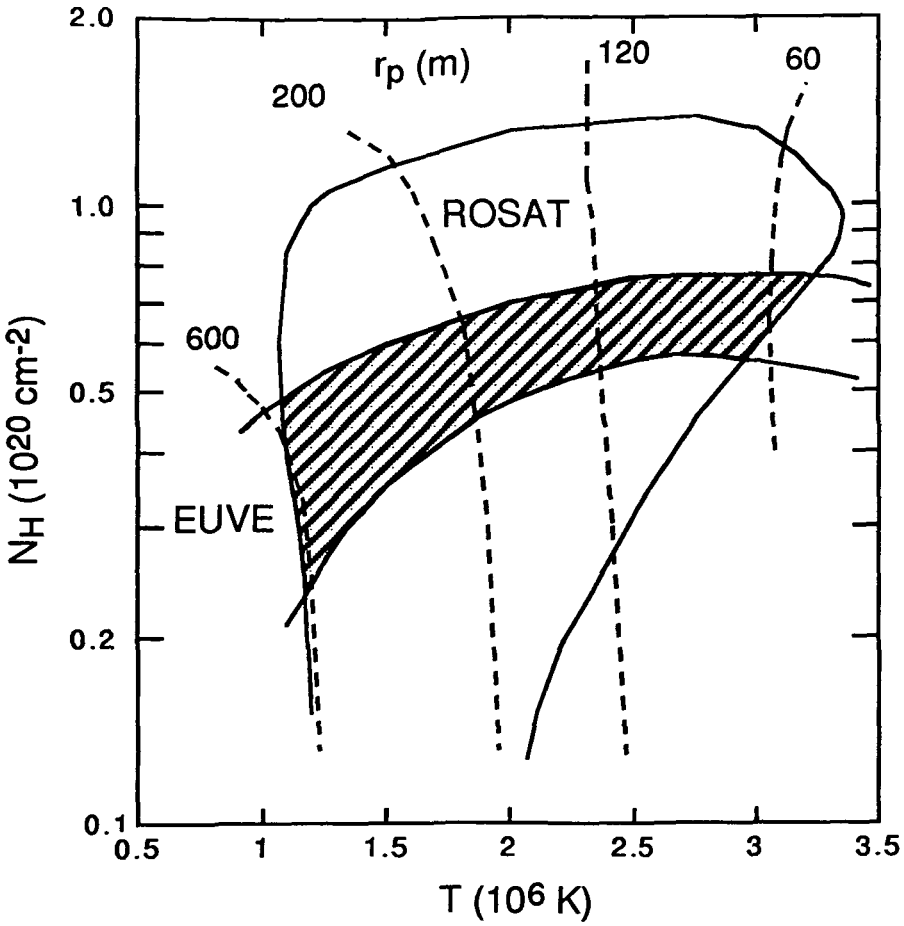
2.0
1.0
0.5
0.2
0.1
N_H (10^{20} cm^{-2})
r_p (m)
200
120
60
600
ROSAT
EUVE
0.5
1
1.5
2
2.5
3
3.5
T (10^6 K)

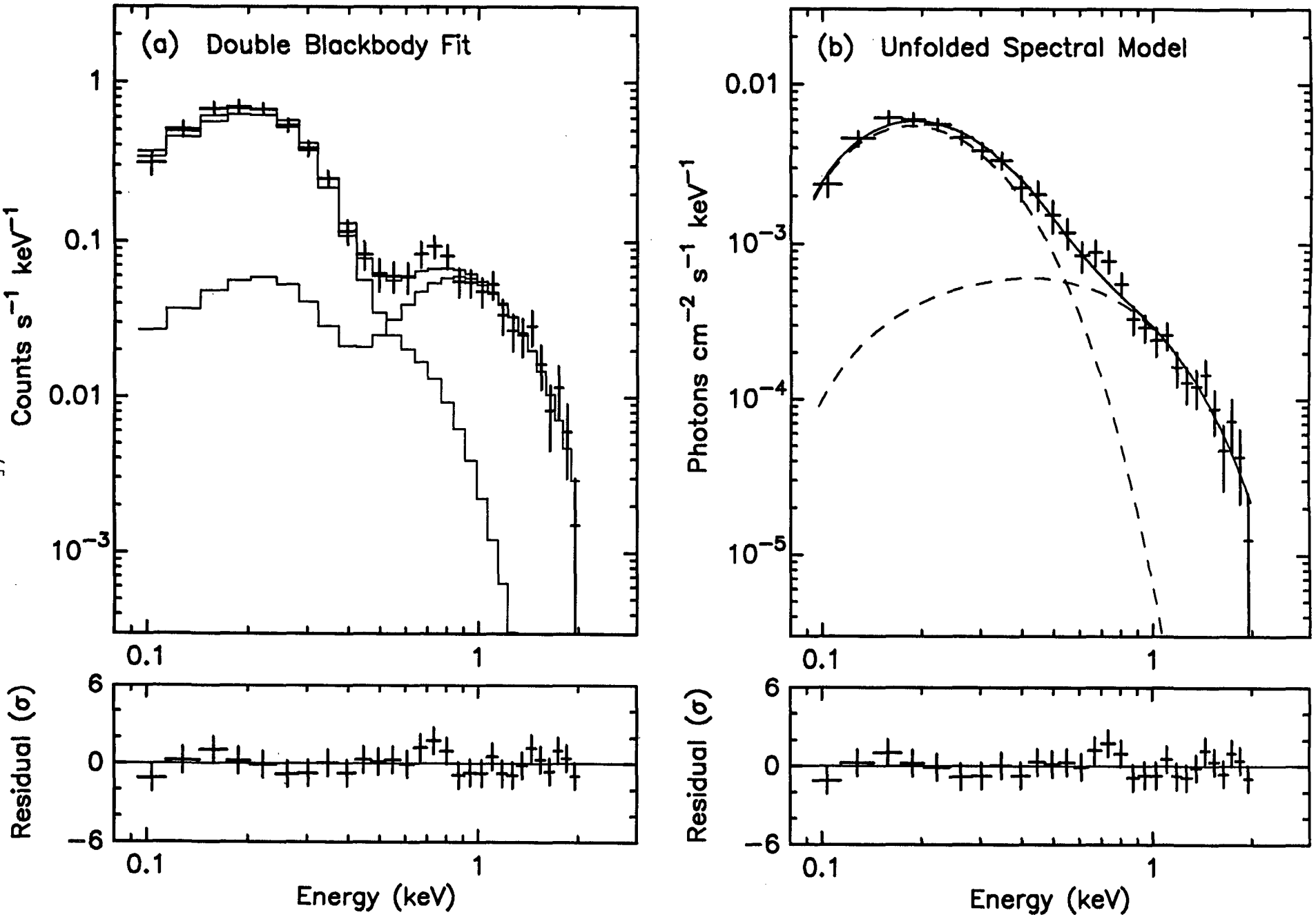
(a) Double Blackbody Fit
Counts s^{-1} keV^{-1}
1
0.1
0.01
10^{-3}
0.1
1
Residual (σ)
6
0
−6
0.1
1
Energy (keV)
(b) Unfolded Spectral Model
Photons cm^{-2} s^{-1} keV^{-1}
0.01
10^{-3}
10^{-4}
10^{-5}
0.1
1
Residual (σ)
6
0
−6
0.1
1
Energy (keV)

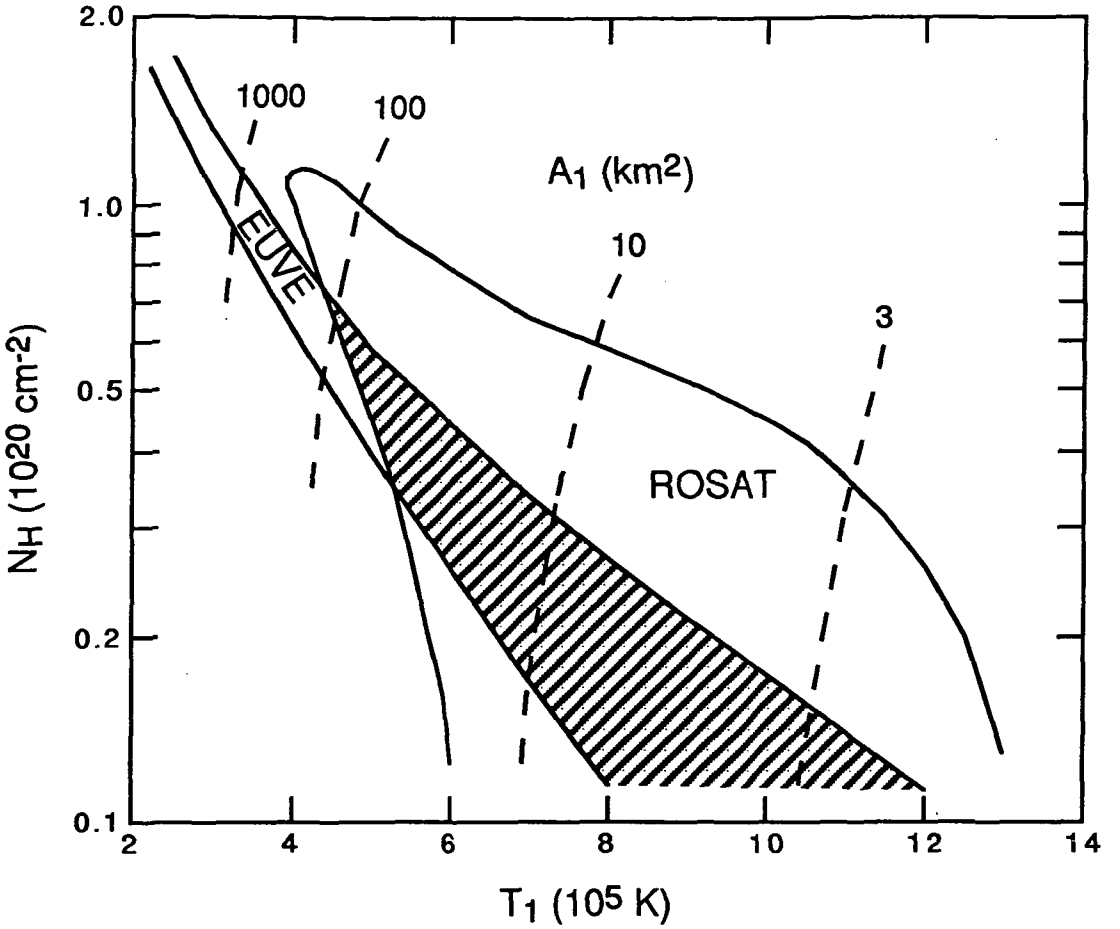
2.0
1.0
0.5
0.2
0.1
2
4
6
8
10
12
14
1000
100
10
3
EUVE
ROSAT
A1 (km2)
NH (1020 cm-2)
T1 (105 K)